

SUPPORTING INFORMATION

1.1 Plot of Gupta Potential and Cutoff

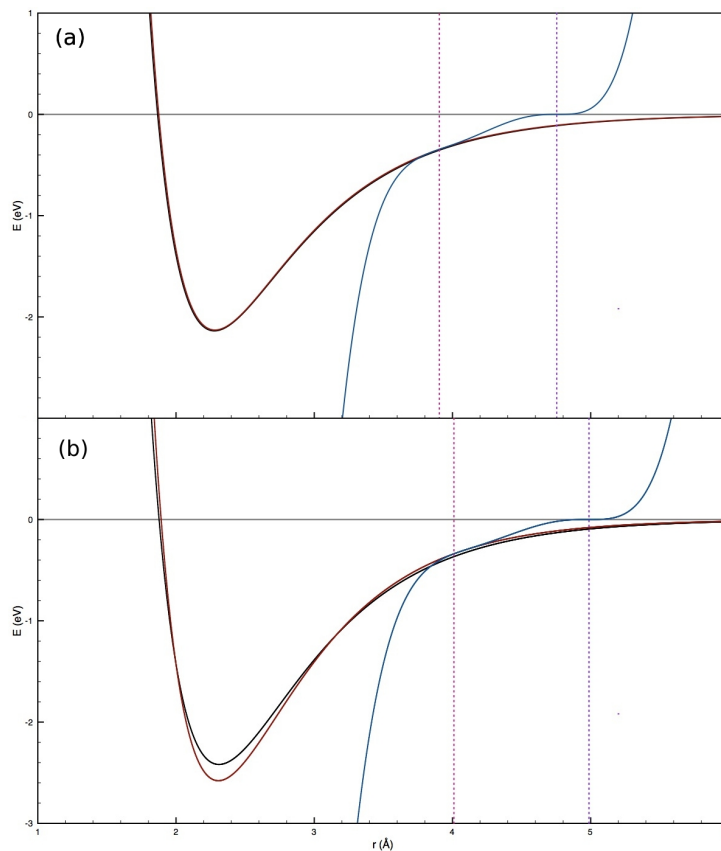


Figure 1.1: Plot of the Gupta Potential function, with different parameters and cutoff in each graph for (a) Pd and (b) Au. Black lines represent the parameters of Cleri and Rosato [1], red lines represent the parameters of Baletto et al. [2], and the blue lines show the polynomial cutoff, with C_s and C_e shown by pink and purple dashed lines, respectively.

1.2 Long Range Cut-off in the Gupta Potential

The parameters used in reference [2] incorporate a long distance cut-off into the potential for atoms further than 2 neighbours distance away ($> \sqrt{2}r$) [3]. The interatomic potential decays with increasing distance and introducing a cut-off speeds up the energy calculations for large clusters.

A 5th order polynomial was introduced, matching that of Baletto *et al.* [2]. For this, a polynomial replacement for the potential that matches the potential function at the cut-off start (C_s), and is zero at the cut-off end (C_e) is derived. The replacement is applied separately to each exponential component of the Gupta potential. Considering the term:

$$V_{ij}^r(r_{ij}) = Ae^{-p(\frac{r_{ij}}{r_0}-1)} \quad (1.1)$$

for $C_s \leq r_{ij} \leq C_e$ we replace the above expression by the following polynomial $p_1(r_{ij})$:

$$V_{ij}^r(r_{ij}) = p_1(r_{ij}) = a_5(r_{ij} - C_e)^5 + a_4(r_{ij} - C_e)^4 + a_3(r_{ij} - C_e)^3 \quad (1.2)$$

where the coefficients a_5 , a_4 , a_3 are chosen to match the function and its first and second derivatives for $r_{ij} = C_s$. For $r = C_e$, $p_1(r_{ij}) = 0$. The form of the polynomial ensures that the conditions on the function and its first derivative are automatically matched for $r_{ij} = C_e$. In the same way, for the term:

$$[V_{ij}^m(r_{ij})]^{\frac{1}{2}} = \zeta e^{-q(\frac{r_{ij}}{r_0}-1)} \quad (1.3)$$

the following polynomial, $p_2(r_{ij})$, is used:

$$[V_{ij}^m(r_{ij})]^{\frac{1}{2}} = p_2(r_{ij}) = x_5(r_{ij} - C_e)^5 + x_4(r_{ij} - C_e)^4 + x_3(r_{ij} - C_e)^3 \quad (1.4)$$

where the coefficients x_5 , x_4 , x_3 are calculated to match the form of the Gupta function. The cut-off parameters used are given in Table 1.1, and included in the potential functions plotted in Appendix 1.1.

Parameter Set <i>II</i>		
	Pd	Au
C_s (Å)	3.890	4.070
C_e (Å)	4.764	4.984
a_3	-5.732×10^{-3}	-8.105×10^{-3}
a_4	-8.477×10^{-3}	-1.110×10^{-2}
a_5	-5.723×10^{-3}	-6.828×10^{-3}
x_3	-3.131	-2.232
x_4	-4.861	-3.258
x_5	-2.157	-1.383

Table 1.1: Cut-offs and polynomial coefficients used for Au and Pd (to 4 significant figures) for parameter set *II*

1.3 Energetic Analysis

1.3.1 Pd_N Clusters

12-Vertex Structures: Icosahedra, Ico-Decahedra and Cuboctahedra.

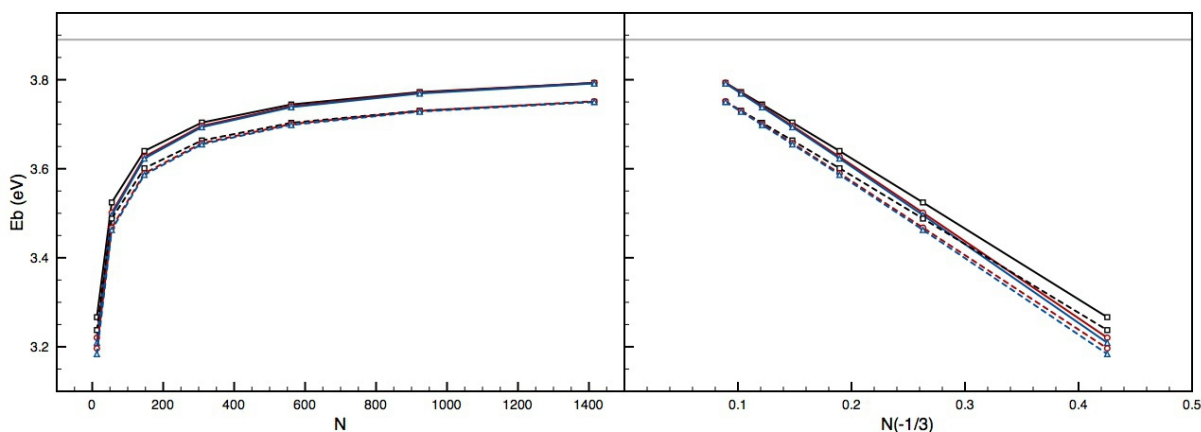


Figure 1.2: Left: Plot of E_b for Pd_N structures against N . Solid lines represent the parameter set *I* of Cleri and Rosato [1], and dashed lines represent the parameter set *II* of Baletto *et al.* [2]. Right: Plot of E_b for Pd_N structures against $N^{-\frac{1}{3}}$. Ih (black squares), I-Dh (red circles) and CO (blue triangles) are shown in both plots; E_{coh} of 3.89 eV [4] is displayed as a grey solid line.

Figure 1.2 plots E_b for Ih, I-Dh and CO structures, with increasing shell sizes k , against N . For $N < 100$, E_b rapidly increases, before levelling off as $N > 500$; this trend is consistent for both parameter sets. Identification between the different structural motifs is energetically difficult, implying that they are all closely competitive in energy at this size. A spacing between trend lines is visible for the two parameter sets: parameter set *I* rises to a higher level than parameter set *II*, before flattening out asymptotically relative to E_{coh} . The difference in gradients between parameter sets *I* and *II* can be identified in the right of Figure 1.2 where an approximation to the E_{coh} is achieved for $N^{-\frac{1}{3}} \rightarrow 0$ when $N^{-\frac{1}{3}}$ is plotted against E_b . Linear extrapolation to 0 for parameter set *I* gives a slightly over-exaggerated E_{coh} (3.92 eV) compared to the experimentally measured value

(3.89 eV [4]), whilst parameter set *II* offers better agreement to this measurement (3.88 eV).

1.3.2 Au_N Clusters

12-Vertex Structures: Icosahedra, Ino-Decahedra and Cuboctahedra.

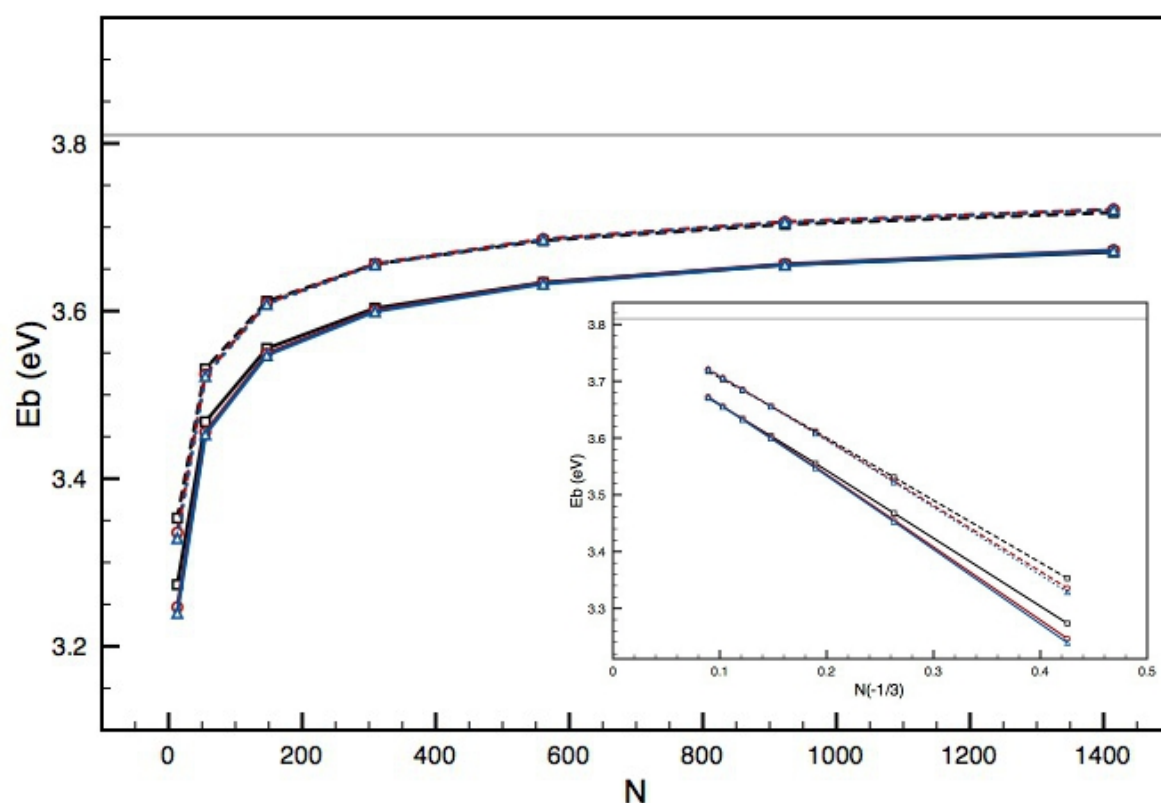


Figure 1.3: Main: Plot of E_b for Au_N structures against N . Solid lines represent the parameter set *I* of Cleri and Rosato [1], and dashed lines represent the parameter set *II* of Baletto *et al.* [2]. Inset: Plot of E_b for Au_N structures against $N^{-1/3}$. Ih (black squares), I-Dh (red circles) and CO (blue triangles) are shown in both plots; the bulk E_{coh} (3.81 eV [4]) is displayed as a grey solid line.

Figure 1.3 compares E_b for the high-symmetry Au_N structures of the Ih, I-Dh and CO geometries. Similar trends to the results of Pd_N are seen with sharply increasing E_b for $N < 100$, levelling out asymptotically towards the bulk E_{coh} value of 3.81 eV [4] as

$N \rightarrow \infty$. Parameter set *II* tends to a higher value of E_b than parameter set *I*, an inverse of the results for Pd_N clusters (Figure 1.2). Attention to the inset, which relates E_b to the bulk limit ($N^{-\frac{1}{3}} \rightarrow 0$), suggests that the parameter set *I* underestimates the extrapolated bulk E_{coh} value (3.77 eV), whilst parameter set *II* does not (3.81 eV).

Structural preferences are difficult to identify in Figure 1.3; we can calculate relative stabilities (ΔE_b) of different geometries with identical nuclearities using:

$$\Delta E_b = E_{b_{Ih}} - E_{b_x} \quad (1.5)$$

where the binding energies of I-Dh or CO can be directly compared with Ih ($E_{b_{Ih}}$) when substituted in for E_{b_x} . Positive values indicate reduced stability, and a negative value indicates increased stability, relative to the Ih; thus ΔE_b is plotted in Figure 1.4 for Au_N clusters.

For parameter set *I* we see intersection of $E_{b_{Ih}}$ at $N = 682$ by $\Delta E_{b_{I-Dh}}$ and at $N = 923$ by $\Delta E_{b_{CO}}$, calculated using a linear fit. For parameter set *II* these intersections of $E_{b_{Ih}}$ are at lower N : 284 and 393 for $\Delta E_{b_{I-Dh}}$ and $\Delta E_{b_{CO}}$, respectively. The values of N for these intersections are much less than found for Pd_N , implying relative instability of the close-packed cluster geometries (Ih, I-Dh) with respect to the crystalline bulk fragments for Au nanoparticles.

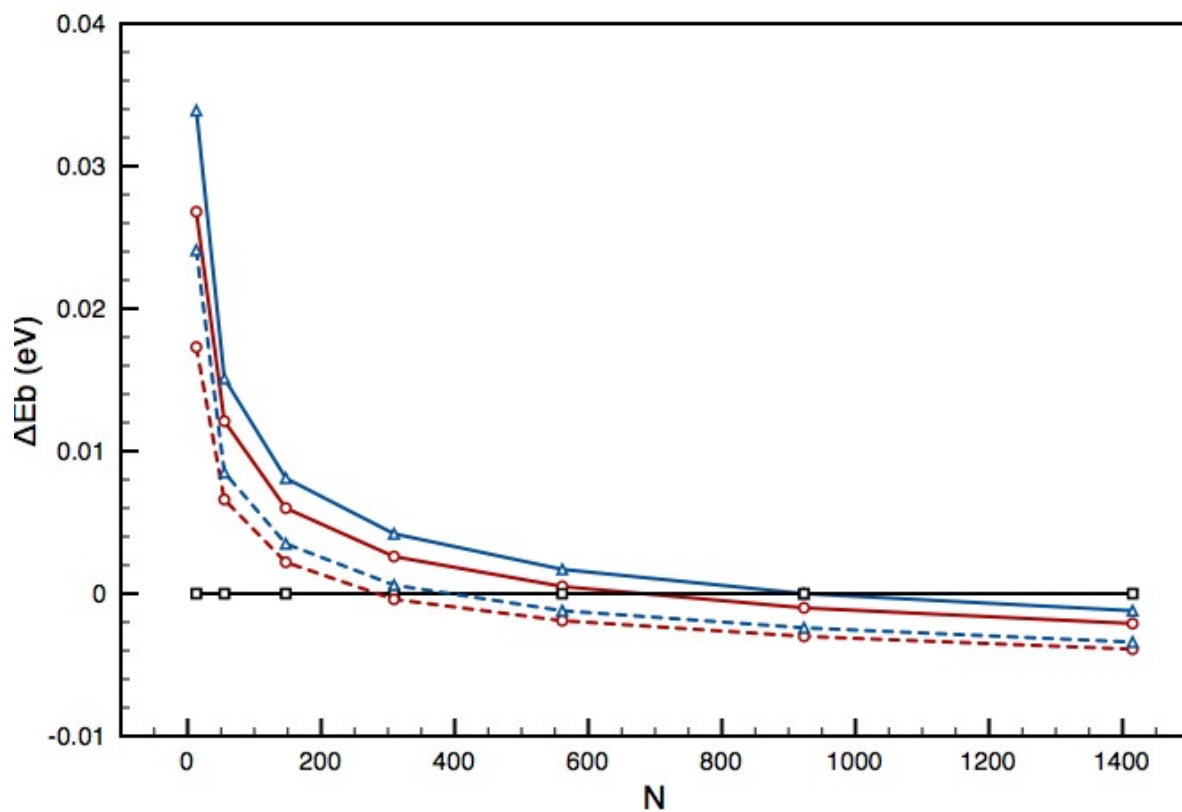


Figure 1.4: Plot of ΔE_b for Ih (black), I-Dh (red) and CO (blue) Au_N structures against N . Solid lines represent parameter set *I* of Cleri and Rosato [1], and dashed lines represent parameter set *II* of Baletto *et al.* [2].

1.3.3 $(\text{Pd}_{\text{core}}\text{Au}_{\text{shell}})_N$ Clusters

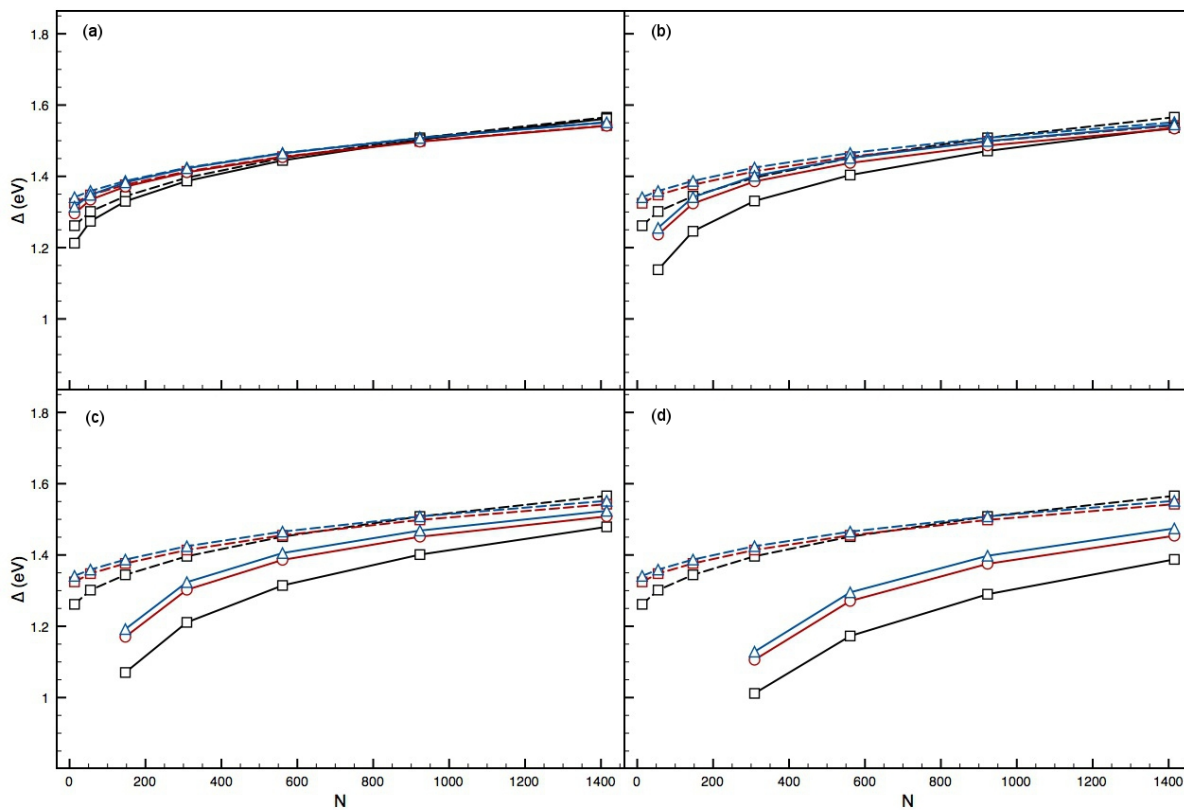


Figure 1.5: Plots of Δ against N for the $\text{Pd}_{\text{core}}\text{Au}_{\text{shell}}$ 12-vertex high-symmetry structures (solid lines), using parameter set I of Cleri and Rosato [1], with cores: (a) Pd_1 (b) Pd_{13} (c) Pd_{55} (d) Au_{147} . Ih (black squares), I-Dh (red circles) and CO (blue triangles) are shown, with Au_N (dashed lines) also plotted.

LIST OF REFERENCES

- [1] F. Cleri and V. Rosato. Tight-binding potentials for transition metals and alloys. *Phys. Rev. B*, 48(1):22–33, 1993.
- [2] F. Baletto, R. Ferrando, A. Fortunelli, F. Montalenti, and C. Mottet. Crossover among structural motifs in transition and noble-metal clusters. *J. Chem. Phys.*, 116(9):3856–3863, 2002.
- [3] R. Ferrando. *Personal Communication*, 2009.
- [4] C. Kittel. *Introduction To Solid State Physics 6th Edition*. Wiley, New York, 1986.